

THE MISMEASURE OF MERGERS: REVISED LIMITS ON SELF-INTERACTING DARK MATTER IN MERGING GALAXY CLUSTERS

DAVID WITTMAN^{1,2}, NATHAN GOLOVICH¹, WILLIAM A. DAWSON³*Draft version January 23, 2017*

ABSTRACT

In an influential recent paper, Harvey et al. (2015) derive an upper limit to the self-interaction cross section of dark matter ($\sigma_{\text{DM}}/m < 0.47 \text{ cm}^2/\text{g}$ at 95% confidence) by averaging the dark matter-galaxy offsets in a sample of merging galaxy clusters. Using much more comprehensive data on the same clusters, we identify several substantial errors in their offset measurements. Correcting these errors relaxes the upper limit on σ_{DM}/m to $\lesssim 2 \text{ cm}^2/\text{g}$, if we follow the Harvey et al. (2015) prescription for relating offsets to cross sections. Furthermore, many clusters in the sample violate the assumptions behind this prescription, so even this revised upper limit should be used with caution. Although this particular sample does not tightly constrain self-interacting dark matter models when analyzed this way, we discuss how merger ensembles may be used more effectively in the future.

1. INTRODUCTION

Dark matter (DM) comprises most of the matter in the universe but little is known about its properties. It has been detected gravitationally, but despite many searches there is as yet no evidence it participates in other known interactions. Perhaps the dominant DM particle model has been the weakly interacting massive particle (WIMP), which is difficult to detect directly. Searches for weak interactions of dark matter with normal matter have rapidly improved in sensitivity, however, and are beginning to rule out interestingly large regions of parameter space (see Klasen et al. 2015, for a review). Another class of models, hidden sector models, posit substantial interactions *between* DM particles even if nongravitational interactions with normal matter are undetectably weak or nonexistent (Feldman et al. 2007; Feng & Kumar 2008; Cohen et al. 2010). Empirical constraints on DM self-interactions rely on astrophysical arguments and are much less stringent than those on interactions between DM and normal matter. Upper limits from astrophysical arguments (e.g., Randall et al. 2008) are on the order of one cm^2/g , or two barns per GeV—twenty orders of magnitude larger than the cross-sections relevant to collider and direct-detection searches.⁴

In other words, if DM particles interact with each other with about the same cross section as neutrons do, this interaction could still have escaped detection to date. This has provided general motivation for efforts to tighten astrophysical constraints on σ_{DM}/m . A more specific motivation comes from measurements of dwarf galaxy and galaxy cluster density profiles, which are suggestive of self-interacting DM (SIDM) with a cross section around $0.1\text{--}5 \text{ cm}^2/\text{g}$ (Boylan-Kolchin et al. 2012; Rocha et al.

2013; Peter et al. 2013; Sand et al. 2008; Newman et al. 2013b,a; Elbert et al. 2015). If true, this would exclude the WIMP model by some twenty orders of magnitude and point the way to some truly new physics. Skeptics, however, point out that these astrophysical environments also contain difficult-to-model baryonic effects that could explain the measured profiles (e.g. Brooks 2014).

A complementary method for probing some types of self-interactions may be to analyze mergers of galaxy clusters (which are mostly DM by mass) as “dark matter colliders.” The well-known Bullet Cluster serves as the best example and yields, at 68% confidence, $\sigma_{\text{DM}}/m < 0.7 \text{ cm}^2/\text{g}$ based on a mass-to-light argument and $\sigma_{\text{DM}}/m < 1.25 \text{ cm}^2/\text{g}$ based on the offset argument described in more detail below (Randall et al. 2008). An ensemble of such mergers could potentially drive this upper limit down enough to confirm SIDM if it exists. Because cluster mergers and galaxy cores probe different velocity scales, such a detection would also characterize the velocity dependence of the interaction and thereby constrain the mediator mass (Loeb & Weiner 2011; Zavala et al. 2013; Kaplinghat et al. 2016). Even if one prefers to view this work as an exercise in excluding SIDM, observations on both low and high velocity scales will be necessary to impinge on the broad class of SIDM models that are naturally velocity dependent (Loeb & Weiner 2011).

Hence there is great interest in the result of Harvey et al. (2015, hereafter H15), who used offsets between galaxies and DM in an ensemble of 30 merging clusters to derive an upper limit of $\sigma_{\text{DM}}/m < 0.47 \text{ cm}^2/\text{g}$ at 95% confidence and $< -0.01 \text{ cm}^2/\text{g}$ at 68% confidence.⁵ This is a dramatic improvement on the previous best constraint from offsets cited above, and thus has already helped drive new constraints on the velocity dependence and therefore the mediator mass (Kaplinghat et al. 2016). Because this dramatic improvement has profound implications for particle models, it warrants further scrutiny. Many of the merging clusters in the H15 sample have been intensively studied individually,

¹ Physics Department, University of California, Davis, CA 95616; dwittman@physics.ucdavis.edu

² Instituto de Astrofísica e Ciências do Espaço, Universidade de Lisboa, Lisbon, Portugal

³ Lawrence Livermore National Laboratory, P.O. Box 808 L-210, Livermore, CA, 94551, USA

⁴ DM cross sections are cited in terms of area per unit mass because the rather than area per particle because astronomers are able to measure the total mass of a collection of DM particles but not the mass per particle.

⁵ The 68% confidence upper limit is not stated directly by H15 but is implied by their Figure 4.

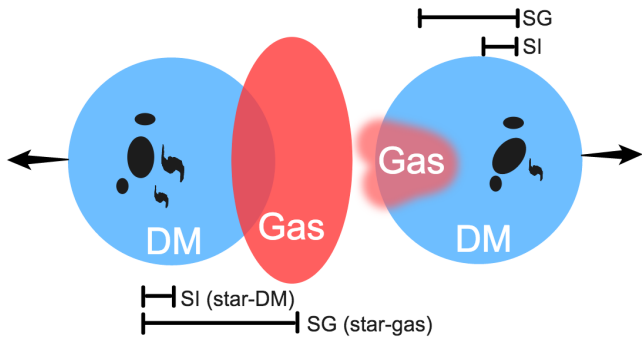


Figure 1. Schematic merger scenario: two subclusters have passed through each other, and the gas associated with each has slowed due to momentum exchange. This is observable as an offset between the star (i.e., galaxy) and gas positions, δ_{SG} . In analogy, any star-DM offset δ_{SI} may be attributed to momentum exchange between the DM halos and thus related to a cross section σ_{DM}/m . Subcluster masses and gas densities may vary considerably.

thus providing independent measurements of numerous DM-galaxy offsets. These independent measurements derive from heterogeneous data sources and analysis methods, but always involve *more* data and analysis than H15 applied to any individual cluster. In this paper we use the more extensive data to reveal substantial errors that, when corrected, greatly loosen the H15 constraint.

The remainder of the paper is organized as follows. Section 2 reviews the basic premise behind the merging cluster technique and outlines the H15 procedure in enough detail to understand which substructures are most highly weighted in the final result. In Section 3 we review the literature on these highly-weighted substructures and either accept the H15 measurement, improve the H15 measurement, or argue that the substructure is unusable for this test. In Section 4 we analyze the updated catalog using the H15 formalism and derive updated SIDM constraints. In Section 5 we discuss the result in the broader context of astrophysical tests of dark matter, and present some concluding remarks.

2. THE MERGING CLUSTER TECHNIQUE

A galaxy cluster consists of gas, DM (constituting the great majority of the mass), and galaxies. When two such clusters fall together, the two sets of galaxies pass through each other with little or no exchange of momentum. The gas clouds, in contrast, exchange momentum and thereby slow down compared to the galaxies. A snapshot of a system soon after pericenter passage, for example the well-known Bullet Cluster, shows the two gas clouds closer to the center of the combined system and the galaxies farther out. The (at least approximately) collisionless nature of dark matter is then demonstrated when gravitational lensing shows that the majority of the mass (and by implication the DM) is coincident with the galaxies rather than the gas (Markevitch et al. 2004). If DM in fact exchanges some momentum in a way analogous to the gas, the DM at this stage of the merger will be located between the galaxies and the gas (Figure 1). The observed DM location thus constrains the DM self-interaction cross-section σ_{DM}/m in this model.⁶

⁶ Other self-interaction models are not well probed by the DM offset but may be probed with other observations; see Section 5.

The same reasoning applies to infall of smaller structures. In the limit of small structures falling into a much more massive structure, Harvey et al. (2014) developed an analytical relation between σ_{DM}/m and the galaxy-DM-gas geometry. Defining the galaxy-gas separation as δ_{SG} (S stands for “star” which is synonymous with “galaxy” in this context), they define a coordinate system starting at the galaxy location and stretching to the gas location. The key observable is the DM displacement along this coordinate system, δ_{SI} , in units of δ_{SG} . This ratio, $\frac{\delta_{SI}}{\delta_{SG}} \equiv \beta$, has a simple analytical relationship to σ_{DM}/m if DM behaves analogously to the gas (see, however, Section 5 for caveats on this analogy). $\beta = 0$ corresponds to collisionless DM, $\beta = 1$ to DM just like baryonic gas, and intermediate values correspond to intermediate cross-sections. H15 averaged over 72 substructures and found $\langle \beta \rangle = -0.04 \pm 0.07$; negative values are unphysical but indicate that the data are in tension with the idea of momentum transfer between the DM halos.

H15 analyzed 72 substructures in 30 systems. To identify the substructures with greatest influence on the ensemble result, note that standard propagation of errors on the ratio $\beta \equiv \frac{\delta_{SI}}{\delta_{SG}}$ yields

$$\sigma_{\beta}^2 = \frac{\sigma_{SI}^2}{\delta_{SG}^2} + \frac{\sigma_{SG}^2 \delta_{SI}^2}{\delta_{SG}^4} \quad (1)$$

H15 adopt an uncertainty of $\sigma_{SG} = \sigma_{SI} = 60$ kpc on each offset measurement. Therefore we can factor this out and write

$$\sigma_{\beta}^2 \propto \frac{1}{\delta_{SG}^2} \left(1 + \frac{\delta_{SI}^2}{\delta_{SG}^2} \right). \quad (2)$$

With inverse-variance weighting, then, the weight of the i th substructure would be

$$w_i \propto \frac{\delta_{SG,i}^2}{1 + \delta_{SI,i}^2 / \delta_{SG,i}^2}. \quad (3)$$

Because $\delta_{SI,i}^2 / \delta_{SG,i}^2 \ll 1$ in most cases, $w_i \propto \delta_{SG,i}^2$ is a good approximation for quick assessment of the importance of a particular substructure in the ensemble. Although H15 multiply Gaussian probability density functions (PDFs) rather than compute a single inverse-variance weighted mean, the effect is the same: substructures with large $\delta_{SG,i}$ predominantly determine the result. This makes intuitive sense, because the ratio $\beta \equiv \frac{\delta_{SI}}{\delta_{SG}}$ is highly uncertain when the denominator is small compared to its 60 kpc uncertainty. Conversely, a large $\delta_{SG,i}$ provides a stable baseline from which to measure the i th ratio, and this results in a narrow PDF, or effectively a large weight for the i th substructure.

Of course, one may question the adoption of $\sigma_{SG} = \sigma_{SI} = 60$ kpc for each offset measurement, because the accuracy of offset measurements may vary substantially from substructure to substructure. Our immediate goal is to identify the substructures with the most influence on the H15 result, so we defer discussion of this point to Section 5.

Table 1 in Section 3.11 lists, in decreasing order, the weight of each substructure as a percentage of the total weight. The list is truncated after 16 substructures comprising 85% of the total weight. Next, we perform a

literature review of these 16 substructures in descending order of weight.

3. LITERATURE REVIEW

We believe this paper will be most useful to the community if it highlights a handful of substantial inaccuracies in H15, rather than revisiting every detail. The following review thus defaults to respecting each H15 measurement unless the literature provides strong evidence to the contrary. Given the heterogeneity of the data, what constitutes “strong evidence” may vary. While acknowledging that this approach could lead to bias (discussed further in Section 5), we are confident that readers will agree with our corrections in most cases. In addition to outright corrections, we will discard substructures for which the matching between gas, DM, and galaxy components is uncertain (e.g., Subsection 3.1). In principle, one may choose instead to model such cases; heavy tails could reflect the probability that the given gas, DM, and galaxy components were never coincident in the past. However, quantifying this probability would be very difficult. Furthermore, we suspect that substructures with such heavy-tailed PDFs would contribute very little to an ensemble constraint. We therefore simply discard such cases.

Throughout this review, keep in mind that H15 used only single-band imaging (not necessarily the same band for each cluster) in their main analysis in order to yield a large and (in some respects) homogeneous sample. Multiband data allow for better selection of lensing sources and better exclusion of foreground galaxies when mapping the light distribution. Multiband imaging and spectra are also necessary to support a strong lensing analysis, which can locate the mass much more precisely than a weak lensing analysis. In fact, each of the highly weighted systems identified in Table 1 has been studied in more detail with some combination of these techniques. The bands observed, the availability of spectroscopy and strong lensing information, and the data processing and analysis choices vary. Nevertheless, we believe it would be wrong to ignore studies that employ far more data and more robust methods than H15 do on the very same merging systems.

Despite the heterogeneity, a few general remarks do apply. First, we do not seek to update the gas positions, because those are unaffected by the use of the additional data and techniques listed above. Of course X-ray analysis choices such as point source removal and smoothing scale are important, but this paper focuses on what can be learned from *additional data*. Second, we generally keep the nominal H15 uncertainty of 60 kpc on each offset, because the papers we draw from generally do not offer a detailed uncertainty analysis on these particular quantities. Third, lensing is sensitive to all forms of mass, not just DM, so the lensing position must be corrected for the gas mass contribution to obtain a position for the DM alone. Papers that supply more accurate lensing positions usually do not supply information necessary to make this correction, so—except in cases where more specific information is available—we adopt the mean H15 correction of -4.3 ± 1.6 kpc (as a reminder, this is in a coordinate system originating at the galaxy position and increasing toward the gas position). The 1.6 kpc uncertainty in the mean of 72 substructures suggests a sample

standard deviation of 13.6 kpc. For most substructures the nominal uncertainty in each offset is 60 kpc so the uncertainty in the gas mass correction is highly subdominant and will be neglected unless otherwise specified.

3.1. Abell 2744 (Northwest)

The top panel of Figure 2 shows the H15 map of this cluster. To orient the reader, each H15 panel portrays one merging system, and each system has at least two substructures. Therefore, at least two independent offsets can be measured from each system (three in this case). In each H15 panel, the red contours indicate the surface brightness of the hot X-ray emitting gas, the green contours indicate galaxy brightness, and the blue contours indicate the mass (primarily DM) distribution as inferred from weak gravitational lensing. H15 draw a triangle connecting the peaks of the three distributions (gas, galaxies, mass) in each subcluster. If DM exhibits a drag force, we expect to find the mass peak between the galaxies and the gas, yielding $\delta_{SI} > 0$. This is referred to as DM “lagging” the galaxies because the gas definitely lags the galaxies (until turnaround; see Section 5). Lateral displacements are considered irrelevant—resulting from measurement error and perhaps other stochastic processes—so δ_{SI} is actually the projection of the galaxy-DM leg of the triangle onto the galaxy-gas leg.

The length of the galaxy-gas leg, δ_{SG} , determines the importance of the substructure in the ensemble analysis (§2); the top panel of Figure 2 shows that the northwest⁷ substructure is by far the most important. This substructure is the most highly weighted in the entire ensemble, with 17% of the total weight, and we focus on it exclusively in this subsection. The corresponding H15 triangle appears to be a long line segment due to negligible lateral displacement. This triangle extends off the HST field of view because the Chandra X-ray Observatory, used to locate the gas, has a much larger field. The galaxy and DM components of this substructure are located on the edge of the HST field, with the DM trailing the galaxies, as predicted by the drag-force model if $\sigma_{DM}/m > 0$.

Merten et al. (2011) performed a detailed strong lensing, weak lensing and X-ray analysis of this cluster, imaging a larger area so the relevant substructure is no longer on the edge of the optical field (bottom panel of Figure 2). They supplemented two-band HST imaging with ground-based VLT and Subaru imaging, as well as 118 spectroscopic redshifts to guide the photometric selection of source galaxies for the lensing analysis. They resolved the western mass peak found by H15 into two distinct mass peaks (labeled NW1 and NW2 in the lower panel of Figure 2), separated by ~ 200 kpc but on the *same* side of the gas. Merten et al. (2011) link both mass peaks to the gas peak via a complicated scenario far outside the Harvey et al. (2014) framework of an infalling subcluster experiencing a small separation between its gas, DM, and galaxy components. Jauzac et al. (2016) developed a detailed strong-lensing mass model using additional data and confirmed the existence of NW1 and NW2, but found them to be coincident with their respective nearby bright galaxies. Meanwhile, Medezinski et al. (2016) analyzed

⁷ H15 and this paper follow the astronomical convention of placing north up and east left on the page.

Subaru and VLT imaging and derived quite different locations for the DM substructures in this system, as well as a different merger scenario. Given these complicated and competing merger scenarios, we cannot be certain that NW1 and/or NW2 were ever united with this particular gas peak. With the gas-galaxy-DM association itself in question, the offsets are not meaningful and the substructure should be omitted from the ensemble. In fact, Harvey et al. (2014) discussed association uncertainty and stated, correctly, that such uncertainty would vanish for substructures with offsets small enough to satisfy their approximation (< 30 kpc). The association uncertainty arises here because $\delta_{SG} \sim 400$ kpc, the largest in the H15 ensemble. Even if more robust associations can be made in the future, this substructure will never satisfy the Harvey et al. (2014) approximation.

Discarding this substructure should *strengthen* the H15 case against SIDM, because this is a very highly weighted substructure that—contrary to the H15 ensemble overall—does have a DM offset in the direction predicted by SIDM. It is worth noting, for illustration purposes only, that the configuration of green, blue, and red contours representing this substructure in the top panel of Figure 2 is to be expected if $\sigma_{DM}/m \approx 1$ cm²/g. Specifically, for this cross section Equation 1 of H15, predicts $\beta \equiv \frac{\delta_{SI}}{\delta_{SG}} = 0.14$, while the (discarded) value here is 0.19. The substructures in H15 more typically exhibit green (galaxy) contours *between* the blue (DM) and red (gas) contours, corresponding to a negative β_i and a negative (unphysical) cross section.

In the remaining subsections of the literature review we will not comment on the impact of each particular correction to the H15 catalog; the foregoing explanation should enable the reader to do so if desired. For Abell 2744, we reiterate that omitting this substructure does nothing to loosen the constraints on σ_{DM}/m , quite the opposite in fact. Our final conclusion that the ensemble constraints are quite loose will owe nothing to the omission of this particular substructure.

3.2. DLSC J0916.2+2951 (South)

Dawson et al. (2012) and Dawson (2013) studied this cluster with two bands of HST/ACS imaging, five bands of deep ground-based imaging, and 634 spectroscopic redshifts to support the background source and galaxy member selection. Figure 3 compares the Dawson (2013) result with that of H15. The southern triangle in the top panel of Figure 3 illustrates the H15 finding that the mass is actually ahead of the galaxies; H15 found $\delta_{SI} = -19$ kpc. The lower panel, from Dawson (2013), shows the lensing mass in a colorscale with galaxy luminosity density overlaid in white contours. The mass is clearly lagging the galaxies; Dawson (2013) found the offset to be +129 kpc based on the lensing peak alone, and +80 kpc after modeling out the gas mass to yield the DM mass alone.

While the H15 uncertainties are large enough to encompass the Dawson (2013) value, the H15 mass position is outside the Dawson (2013) 2σ confidence ellipse (the larger dashed ellipse). Because the Dawson (2013) value is supported by multiband selection of lensing sources and member galaxies, backed up by extensive spectroscopy, we adopt $\delta_{SI} = 80$ kpc.

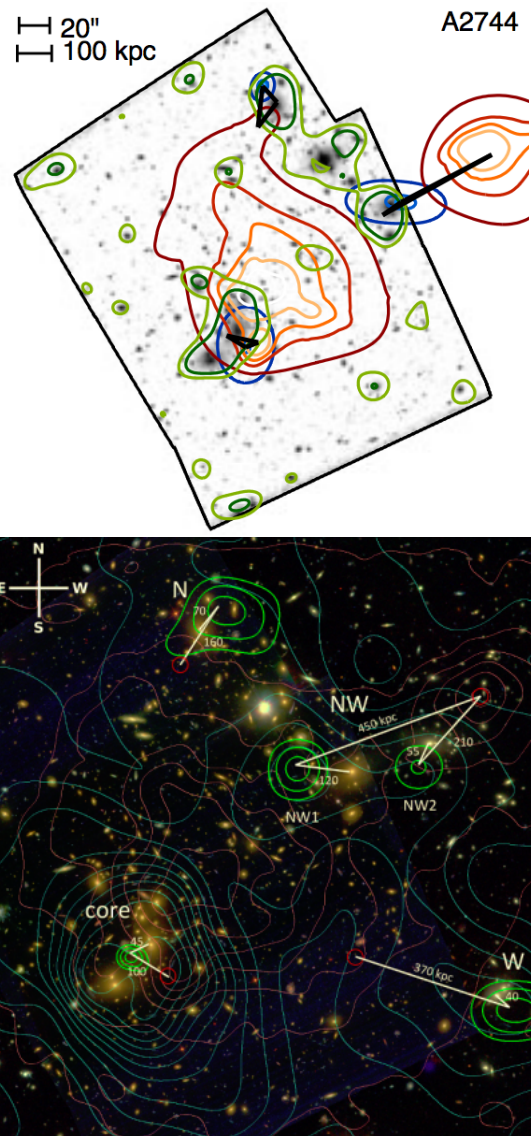


Figure 2. *Top:* View of Abell 2744 from H15. In all panels from H15, X-ray (gas) contours are reddish, green contours indicate visible light, and blue contours indicate mass inferred from gravitational lensing. In the highly weighted western subcluster the heavy black line indicates nearly collinear alignment of galaxies, DM and gas. *Bottom:* map from the more detailed analysis of Merten et al. (2011), with x-ray (red), lensing (cyan), and confidence contours for lensing peak locations (green, with 0.3σ , 1σ , 2σ contours). The H15 mass peak is now resolved into two peaks (NW1 and NW2), contradicting the H15 assumption of simple infall of a gas-DM-galaxy substructure.

3.3. Abell 520

All five of the Abell 520 substructures identified by H15 are in the top 16 substructures by weight, so we review the entire system at once. In the top panel of Figure 4 we label the H15 substructures for reference below; the bottom panel shows a thorough multiband lensing analysis from Jee et al. (2014a). Clowe et al. (2012) also performed a detailed lensing analysis; their map differs from that of Jee et al. (2014a) primarily in being less smooth and thereby displaying more substructure. Although much more could be said about these two detailed analyses and this complex system, our points here are limited to examining the validity of the H15 substructure.

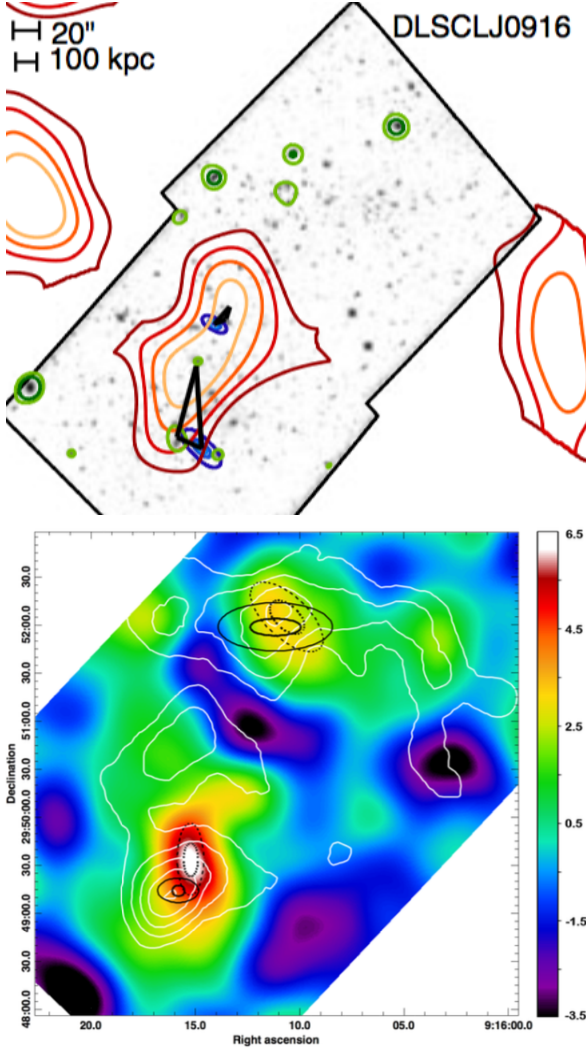


Figure 3. *Top:* View of DLSCL J0916 from H15. In the highly weighted southern subcluster, H15 find the mass to be ahead of the galaxies ($\delta_{SI} = -19$ kpc), corresponding to a negative σ_{DM}/m . *Bottom:* the more detailed analysis of Dawson (2013), with mass in colorscale and galaxy luminosity density in white contours. In the south, the galaxy position agrees with that of H15 and thus serves as a reference point for comparing the two panels; Dawson (2013) find the mass to be trailing the galaxies. Solid (dashed) ellipses are 68% and 95% confidence intervals for the galaxy luminosity (mass) centroid.

tures and offsets.

Substructure 1: this northern subcluster is the most highly weighted of the five, with about 10% of the total weight of the H15 sample. This substructure is consistently identified and located by Jee et al. (2014a) and Clowe et al. (2012). Their maps qualitatively agree with H15, so we adopt the H15 offset.

Substructure 2: this is the second most highly weighted substructure in the system, with about 5% of the total weight of the H15 sample. However, there is no clear gas peak in the area. A secondary issue is that the mass peak presented by H15 does not correspond to a mass peak in Jee et al. (2014a). It does correspond to a mass peak in Clowe et al. (2012); H15 note that they were guided by the literature when locating substructures in Abell 520, but they did not note the controversy surrounding the existence of some of the substructures in Abell 520, in-

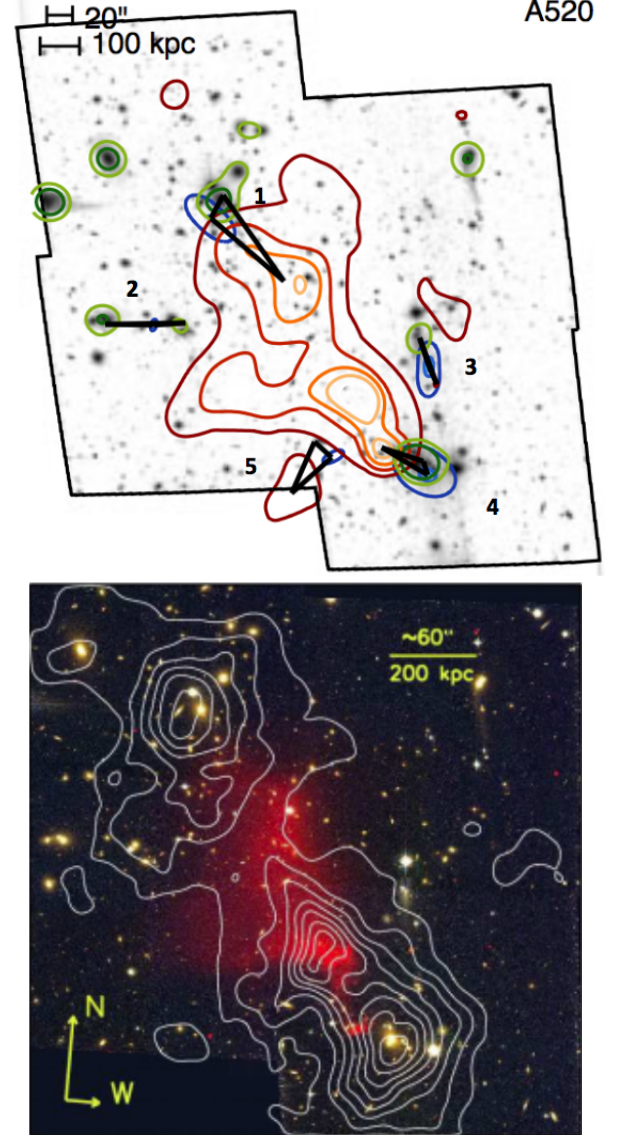


Figure 4. *Top:* H15 analysis of Abell 520. The numerical labels are our annotation, to clearly link to descriptions of substructures in the text. *Bottom:* multiband lensing analysis from Jee et al. (2014a), with X-ray in redscale and lensing contours in white.

cluding this one. Regardless of the reality of the mass peak, the absence of a gas peak prevents us from defining any gas-star-DM geometry. We therefore recommend omitting this putative substructure from the catalog.

We will see several more examples where the X-ray peak is not apparent in the H15 figure, so we address the issue more generally here. Technically the gas peak in this substructure is not absent but merely at too low a signal-to-noise ratio (S/N) to appear on the H15 panel, which shows only a handful of contour levels. However, we see no indication of a diffuse X-ray source at this location in other presentations of the X-ray data, for example the pixelized redscale in the Jee et al. (2014a) panel, or the detailed X-ray analysis of this system presented by Markevitch et al. (2005). H15 automatically matched gas, galaxy, and DM peaks by searching for the nearest peak, so we suggest that this algorithm simply found a very low S/N local X-ray maximum. Many such local maxima must exist due to point sources, which cannot

always be identified and removed. Elsewhere in Abell 520 (Substructure 3, below) an unremoved point source clearly provides the H15 X-ray peak, so it is likely that the same mishap occurs with fainter (and more numerous) point sources not visible in the figures. Point sources are likely in the background, not the cluster, and in any case their emission does not trace the gas, so such peaks cannot be used to define substructures and offsets.

Substructure 3: the “gas peak” is very likely an X-ray point source. In the H15 panel of Figure 4, the gas peak contour has an extremely small angular extent, and the corresponding Jee et al. (2014a) panel shows an X-ray point source there. (A similar point source appears in the northwest corner of both panels, buttressing the contention that H15 did not effectively remove X-ray point sources from this field.) Furthermore, the H15 mass peak does not correspond to a peak in Jee et al. (2014a) nor in Clowe et al. (2012). Finally, most of the light in the green contour is actually a streak from the bright star to the north rather than galaxy light—this is more easily seen by comparison to the lower panel of Figure 4, which has fewer overlays. The streak is probably caused by some combination of CCD bleeding, charge transfer inefficiency, and the star being near the chip gap, which makes its effects on the neighboring chip more difficult to remove. The appearance of this streak thus varies greatly depending on the specifics of the image processing, for example it is absent in Clowe et al. (2012) and in most press release images. H15 kindly allowed us to inspect a higher-resolution version of their image, and the streak begins further north and contains more total light than in the Jee et al. (2014a) image. Without the streak, it is unlikely that H15 would have identified a galaxy luminosity peak here.

In summary, the literature confirms neither the gas, the galaxy luminosity, nor the lensing mass peak for this substructure, so we remove it from the ensemble analysis.

Substructure 4: along with Substructure 1, this is one of the two widely confirmed substructures in the system, and the H15 locations are consistent with previous work in the literature. We adopt the H15 offset. Note that this substructure carries substantially less weight than the northern substructure—at 1.6% of the total weight, it is the least weighty substructure in our literature review.

Substructure 5: any X-ray emission in this area is too faint to be seen in the Jee et al. (2014a) panel of Figure 4. The less highly processed X-ray image of Markevitch et al. (2005) shows what is possibly a local maximum at this location, but it is difficult to argue that it represents a separately identifiable gas concentration. Furthermore, the visible-light peak consists of a single galaxy, and Jee et al. (2014a) show a dearth of mass at the location of the H15 mass peak. Clowe et al. (2012) show what is possibly a mass peak in the general area, but on the opposite side of the light peak compared to H15. Given the lack of confirmation in the literature, we recommend removing this putative substructure from the ensemble analysis.

We emphasize that these recommendations do not hinge on the adoption of the Jee et al. (2014a) lensing map over that of Clowe et al. (2012), which shows more substructures. For each of the three H15 substructures we recommend omitting, there are serious doubts about the reality of the X-ray and/or galaxy peak, regardless of

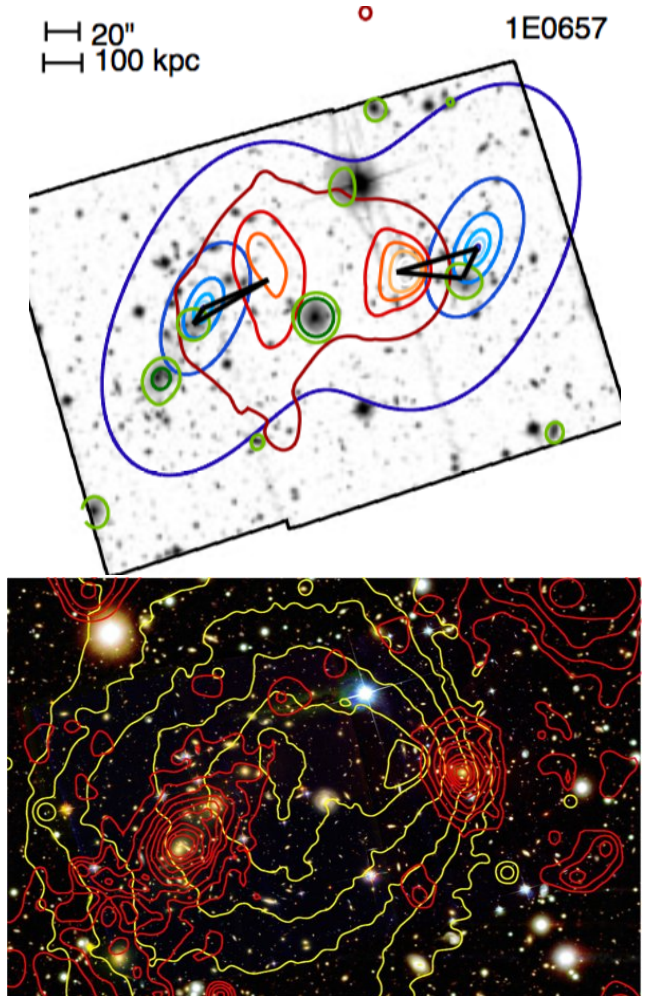


Figure 5. *Top:* View of the Bullet Cluster from H15. *Bottom:* maps from the more detailed analysis of Bradač et al. (2009), with mass contours from strong and weak lensing in red, and X-ray in yellow. The H15 lensing position for the western subcluster, putting the mass ahead of the galaxies, is highly excluded based on this more detailed analysis.

the reality of the lensing peak. Only one of the omitted H15 substructures (number two) definitely corresponds to a lensing peak that appears in Clowe et al. (2012) but not in Jee et al. (2014a). Even if we adopt the Clowe et al. (2012) lensing map and grant the reality of this mass peak, it is clear from Figure 4 that there is no significant gas peak and that the matching to a galaxy peak is ambiguous.

3.4. 1E0657-56 (the Bullet Cluster)

Both substructures in this system are highly weighted in the H15 analysis: the eastern (main) subcluster ranks fourth with 6.1% of the total weight, and the western (bullet) subcluster ranks ninth with 3.8% of the total weight. These weights reflect how well the gas and galaxies are separated in this system, clearly establishing the baseline to which the galaxy-DM separation must be compared. This cluster has been extensively studied; the combined strong and weak lensing analysis of Bradač et al. (2009) is shown in the bottom panel of Figure 5.

East: the H15 lensing contours do not match Bradač et al. (2009), who show many lensing contours tightly wrapped around the galaxies with essentially zero offset.

Furthermore, the Bradač et al. (2009) lensing contours are much more prominent around the brighter of the two brightest galaxies in this subcluster, whereas H15 put all the mass near the fainter of the two. Given that the Bradač et al. (2009) picture is supported by a detailed strong lensing analysis, the H15 lensing contours are simply not credible. The Bradač et al. (2009) shows no discernible offset, so we adopt an offset of zero. The following paragraph contains more details for those with a special interest; most readers are encouraged to skip to the West substructure.

Given that H15 split the galaxy light into two peaks and connected the gas to the nearer and lesser peak, a narrow interpretation of our task is to find the position of the DM *associated with this particular local maximum in the light distribution*. Even so, the Bradač et al. (2009) map does not support the 40 kpc offset to the northwest shown by H15; if anything, there may be a small offset in the opposite direction. This also raises issues of how finely to split substructures and how to match them; it seems implausible to assign all the gas to the second-brightest galaxy, for example. To keep this literature review focused, we defer those questions to Section 5.

West: this is similar to East in that Bradač et al. (2009) show many lensing contours tightly wrapped around the brightest cluster galaxy (BCG). With a single dominant BCG, H15 no longer split the galaxy distribution, so comparison between the two papers is more straightforward than for the East. The BCG is the best point of reference for comparing the maps, because H15 draw a green (starlight) contour around it. H15 find the mass to be peaked to the northwest of this, with an offset of -31 kpc when projected onto the galaxy-gas vector. This position is highly excluded by the mass map of Bradač et al. (2009). Randall et al. (2008) explicitly analyzed the offset between galaxy and mass centroids and found the mass to be 25 ± 29 to the west, that is, along the merger axis toward the gas.

Each of these updated lensing offsets must be corrected for the gas mass contribution as described at the start of this section. This is the system least likely to need such a correction, because the lensing contours are so clearly separated from the bulk of the gas. Nevertheless, to avoid any possible bias toward SIDM we apply the mean H15 correction to each substructure. This correction leads to a final offset of $\delta_{SI} = -4.3$ kpc in the East, and 21 kpc in the West.

3.5. MACS J2243.3-0935

Both subclusters in this system have substantial weight (4.9% for the east and 3.4% for the west), so we treat them together. The bottom panel in Figure 6 is from von der Linden et al. (2014), who performed a careful weak lensing analysis supported by 10 bands of photometry. In addition, Schirmer et al. (2011) analyzed a larger field including this system, using five-band CFHT/Megaprime imaging in good seeing. They used photometric redshifts to support source selection and member galaxy identification, and further used 190 spectroscopic redshifts to finely calibrate the photometry and obtain ~ 0.03 rms redshift uncertainty. Their maps cover a much broader field at lower resolution and so are not presented here, but they confirm the von der Linden et al. (2014) picture of a single smooth, round, high S/N mass concentration

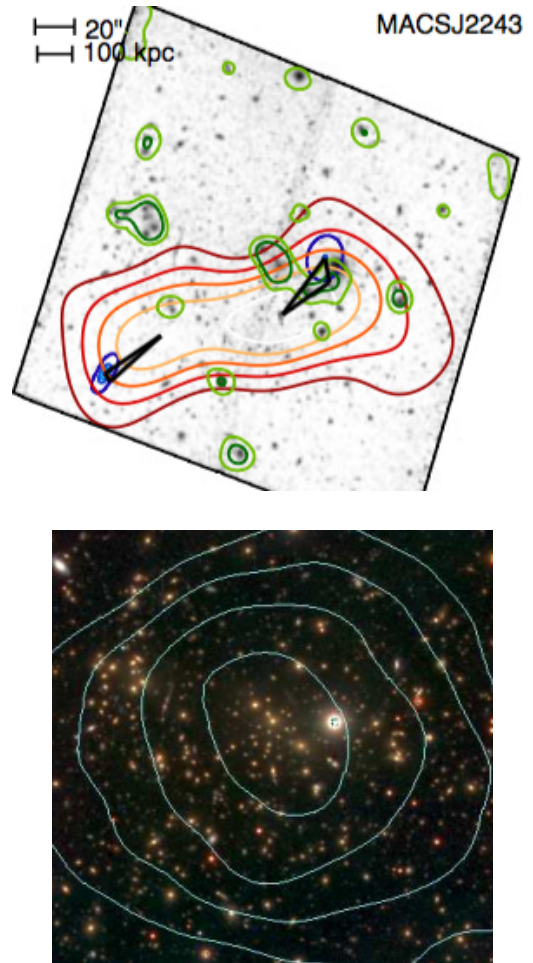


Figure 6. *Top:* View of MACS J2243 from H15. *Bottom:* mass contours from von der Linden et al. (2014).

centered on the galaxy concentration that appears at the center of the bottom panel of Figure 6.

The top and bottom panels of Figure 6 look rather different at first, so we advise the reader to focus first on the bright star that dominates the bottom panel. This star is also the brightest (most black) object in the upper panel, but there much of it is obscured by the blue, green, and red contours that run over it. There are two dense concentrations of galaxies, one immediately to the left (east) of this star and the other farther east. These galaxy concentrations, with heavy green contours in the H15 map, are useful points of reference when comparing the maps, but in fact neither is used by H15 as a substructure. We consider the H15 substructures individually below.

East: the triangle representing this substructure is seen at the lower left of the H15 image. However, there is no convincing concentration of galaxies at this position in either panel of Figure 6, nor in Schirmer et al. (2011). Furthermore, neither von der Linden et al. (2014) nor Schirmer et al. (2011) find a lensing peak here. The absence of confirmation in more extensive data sets suggests that the H15 lensing peak is spurious. We omit this substructure from the remaining analysis.

West: the color image from von der Linden et al. (2014) demonstrates that the H15 luminosity peak just south of the bright star cannot be due to *galaxy* luminosity. Although H15 implemented an algorithm for removing

stars before smoothing the visible light distribution, the most plausible explanation for this H15 luminosity peak is residual light from the exceptionally bright star. The green contours to the east of the bright star in the H15 panel represent a more valid galaxy luminosity position. This yields $\delta_{SI} \approx 0$ because the galaxy-lensing offset is perpendicular to the galaxy-gas offset. The following paragraph contains more details for those with a special interest; most readers are encouraged to skip to the next subsection.

For completeness, we note that the lensing maps also disagree: the von der Linden et al. (2014) lensing map is clearly centered on the galaxies rather than on the blue H15 contour above the bright star. The von der Linden et al. (2014) map (confirmed at lower resolution by Schirmer et al. 2011) suggests that the offset between lensing and galaxy luminosity is approximately zero. In other words, with the correct luminosity position the offset is roughly zero regardless of the lensing map we adopt. The associated uncertainty is difficult to quantify from the information in von der Linden et al. (2014) and Schirmer et al. (2011), but the default H15 value of 60 kpc is a reasonable estimate. The gas mass correction is small compared to this uncertainty, but we apply it nevertheless to avoid bias in the ensemble. This yields $\delta_{SI} = -4.3$ kpc after gas mass correction.

3.6. ZwCl 1358+62 (East)

Zitrin et al. (2011) performed a strong-lensing analysis of this cluster using deep six-band HST/ACS imaging. They found 23 images of eight different sources to support the construction of a mass model. The resulting critical curves are shown on top of a color ACS image in Figure 3 of Zitrin et al. (2011), repeated here as the bottom panel of Figure 7. The H15 panel shows X-ray contours strongly peaked on the BCG; this system also has a beautiful low surface brightness X-ray tail, not visible here, extending along with the galaxies to the south-southeast.⁸ This strongly suggests a merger axis along a south-southeast direction. The Zitrin et al. (2011) strong-lensing mass reconstruction matches the mass distribution one would expect in this situation: elongated toward the south and with a secondary peak corresponding to the southern galaxies. In this context, the H15 weak-lensing finding of a large mass to the east, and none to the south, is difficult to explain.

The putative H15 mass is just off the eastern edge of the Zitrin et al. (2011) map, so there remains some possibility that the H15 mass peak is real. If so, there is essentially no associated gas peak. The X-ray has nearly uniform (low) surface brightness, but H15 apparently identified a local maximum and automatically matched it to a peak in their mass map much further to the east. There is no plausible connection between the X-ray tail and this putative substructure in the east, as the X-ray morphology indicates a merger along an axis from the south-southeast to the north-northwest. Finally, the associated luminosity peak is not convincing either, consisting of one or two galaxies. We recommend omitting this substructure from the sample.

Observant readers may notice that the Zitrin et al.

⁸ See the H15 press release image at http://chandra.harvard.edu/photo/2015/dark/dark_zwc1358.jpg.

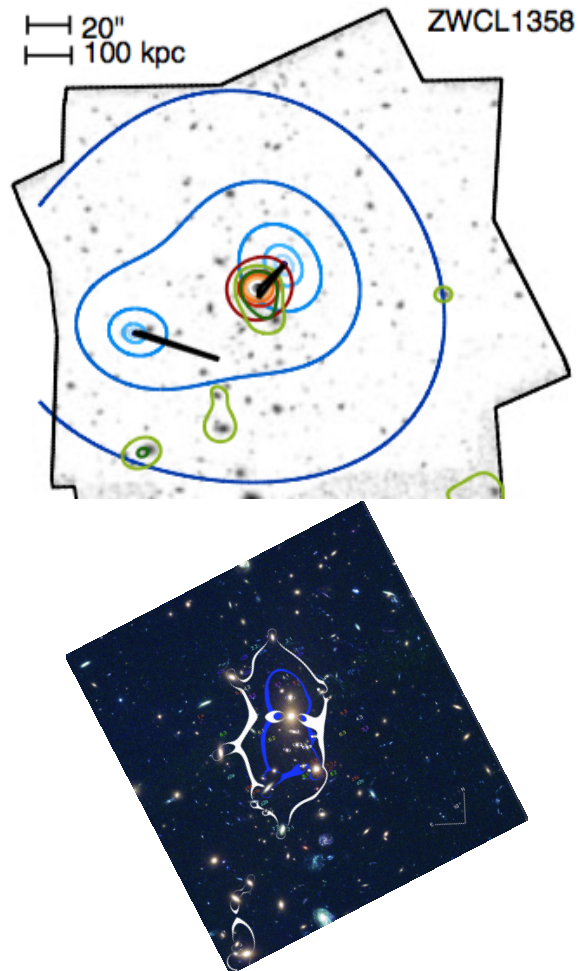


Figure 7. *Top:* View of ZwCl 1358 from H15. *Bottom:* lensing critical curves from Zitrin et al. (2011), showing a secondary mass peak to the south rather than to the east as shown by H15.

(2011) and H15 results also disagree in the main part of the cluster, near the X-ray peak. We do not examine this further because this substructure carries only 0.006% of the total weight of the sample due to the small offset between X-rays and galaxies. Also, readers wishing to search the literature on this cluster should be aware that it has several names, including but not limited to ZwCl 1358.1+6245, MS 1358.4+6245, MACS J1359.8+6231, and RXC J1359.8+6231.

3.7. MACS J0025.4-1222 (West)

Figure 8 compares the H15 map with that of Bradač et al. (2008), who used strong and weak lensing supported by deep three-band HST and five-band Subaru imaging. Here we are concerned only with the western substructure, on the right of each panel. The Bradač et al. (2008) mass peak (red contours) matches the position of the luminosity contours in either panel, but not the H15 mass contours. In fact, the cyan cross in the Bradač et al. (2008) panel gives the 1σ error bar on the mass position, showing that the H15 position is excluded at about the 3σ level. However, Bradač et al. (2008) still find the mass to be slightly ahead of the galaxies, in large part because their galaxy position is a bit further back than the H15 position.

According to Table 2 of Bradač et al. (2008), the

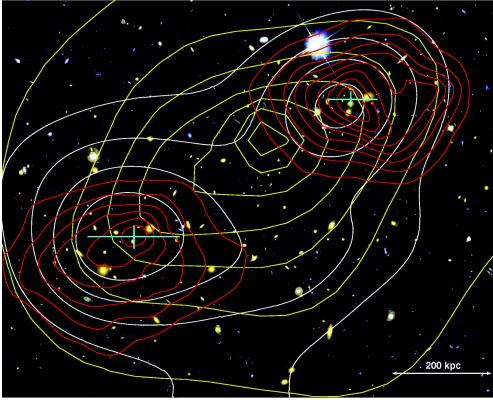
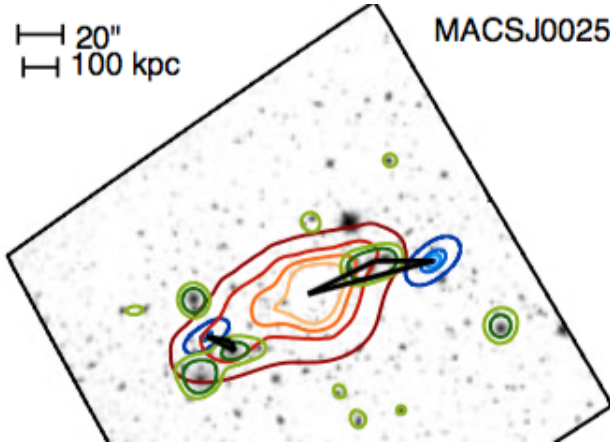


Figure 8. *Top:* View of MACS J0025 from H15. *Bottom:* lensing (red), X-ray (yellow), and *I*-band light (white) contours from Bradač et al. (2008). Crosses show 1σ uncertainties on the mass positions.

galaxy-mass offset is -4.4 arcsec (-29 kpc). With the mean H15 correction for gas mass, the final value for δ_{SI} is -33 kpc. This is a substantial change from the H15 value of -151 kpc.

3.8. ACTCL J0102-4915 (*El Gordo*, North)

Figure 9 compares the H15 analysis with that of Jee et al. (2014b), who used four-band imaging in conjunction with the photometric redshift catalog of Menanteau et al. (2012) and 89 spectroscopic redshifts (Sifón et al. 2013) to obtain clean background source selection—a particularly important issue when the lens is itself at fairly high redshift ($z = 0.87$). Jee et al. (2014b) found two mass concentrations roughly coincident with the northwest and southeast galaxy concentrations, and found no other mass concentrations in the area. H15 differ starkly in finding a mass concentration not at the northwest galaxy location, but ~ 700 kpc away. The H15 location is remarkably coincident with the gap between detectors in the Advanced Camera for Surveys (ACS) data used by H15. We suggest that this is a spurious lensing peak related to the difficulty of cleaning data in or near the gap. We find further support for this suggestion in the strong lensing analysis of Zitrin et al. (2013), whose critical curves are consistent with the mass distribution of Jee et al. (2014b) but not that of H15.

Other aspects of the northern H15 substructure are problematic as well. The H15 galaxy position does not look like a galaxy overdensity in color images, and even

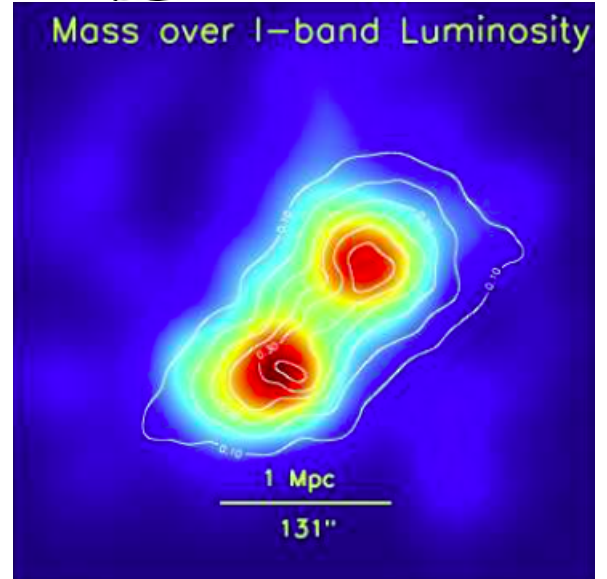
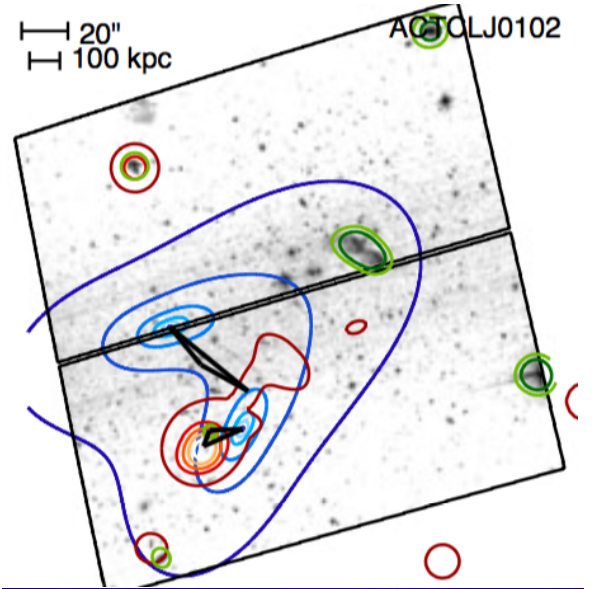


Figure 9. *Top:* H15 analysis of ACTCL J0102 (*El Gordo*). *Bottom:* lensing contours (white) and galaxy luminosity density (colormap) from Jee et al. (2014b). There is severe disagreement over the location of the northern lensing peak. The Jee et al. (2014b) location is coincident with the galaxies, while the H15 location appears to be an artifact of the ACS chip gap.

the H15 figure panel lacks green contours at this location (the middle vertex of the triangle). Furthermore, the H15 triangle suggests a southwest-northeast merger axis, but an overwhelming variety of other evidence (all of the above-cited papers plus the radio relics presented in Lindner et al. 2014) supports a southeast-northwest merger axis; nowhere in the extensive literature on *El Gordo* is there any evidence for a southwest-northeast merger axis.

In summary, H15 have incorrectly characterized the northern substructure. We may be able to infer δ_{SI} from Jee et al. (2014b) and/or Zitrin et al. (2013). However, there is no gas peak associated with the northwest subcluster. The detailed X-ray map of Menanteau et al. (2012) shows a large region of tenuous gas, but no identifiable peak. In this situation, even a peak-agnostic al-

gorithm such as a centroid would have a very large associated uncertainty, implying that this substructure would have little influence on the ensemble. Therefore, we recommend omitting this substructure from the ensemble.

3.9. MACS J0417.5-1154 (North)

von der Linden et al. (2014) performed a weak lensing analysis of this cluster using three-band Subaru imaging. Their lensing map has rather low resolution and so is not presented here, but it does show the same southeast-northwest axis as the H15 lensing map (Figure 10). The galaxy distribution and X-ray morphology follow the same axis, so there is no reason to doubt the H15 lensing map.

Nevertheless, this substructure is worth discussing to illustrate some ambiguities facing next-generation analyses of this sort. First, as suggested by the H15 X-ray contours, the X-ray morphology (Mann & Ebeling 2012) shows a long ridge to the northwest with no peak other than the main peak identified with the southern subcluster. H15 presumably identified a minor local maximum as the subcluster gas location, but this is a somewhat arbitrary location along a long smooth ridge. Without a clear X-ray peak along this ridge, there is great uncertainty in the galaxy-gas vector and therefore in the weight this substructure should receive as well as in the projection of the DM-galaxy vector onto the galaxy-gas vector. Second, the H15 DM peak appears midway between two luminosity peaks. The H15 matching algorithm chose the luminosity peak nearer the putative gas peak, yielding $\delta_{SI} = 2$ kpc after projection onto the galaxy-gas vector). Automatically matching the nearest peak may introduce a bias: if the brighter luminosity peak had been adopted, this substructure would have different implications for SIDM, with $\delta_{SI} \approx 50$ kpc over a longer (~ 200 kpc) galaxy-gas baseline providing a great deal of weight. Or, with more smoothing of the light, the luminosity location would be intermediate and the implication for SIDM would be intermediate. This exposes the need to develop methods less sensitive to smoothing scale, or at least an objective way to optimize the smoothing scale in each system.

3.10. ZwCl 1234+2916 (West)

This cluster illustrates the level of agreement we would expect for independent investigations using overlapping data. Figure 11 compares the H15 analysis with that of Dahle et al. (2013), who used two-band VLT imaging as well as the extremely deep ACS imaging in a third band (the data used by H15). The Dahle et al. (2013) lensing contours (in red) agree with H15 in showing each mass concentrations slightly to the north and, in the east-west direction, slightly closer to the center of the system compared to the corresponding galaxies. Here we are concerned with the western substructure. Although H15 put the mass concentration slightly farther north than do Dahle et al. (2013), this displacement is nearly perpendicular to the merger axis and so has little effect on δ_{SI} . Dahle et al. (2013) do not list a value of δ_{SI} , but measurements of their map yield ≈ 10 kpc, close to the H15 value of 28 kpc. Although the agreement is not perfect, this level of variation is to be expected in independent analyses. We retain the H15 offset.

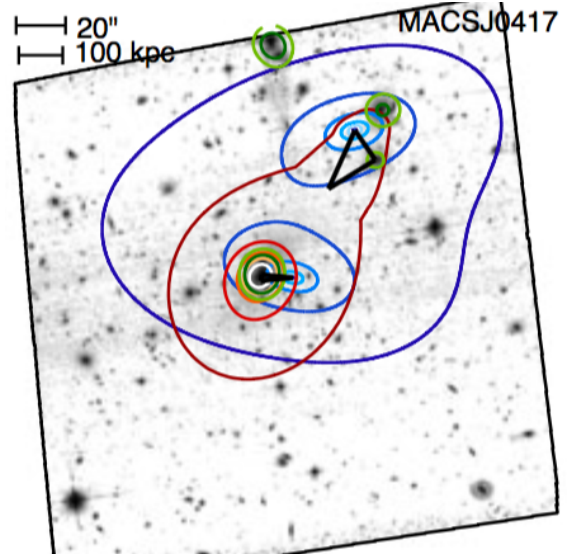


Figure 10. H15 analysis of MACS J0417. Only the northern subcluster is highly weighted and considered here. The X-ray morphology there consists of a long ridge rather than a peak. The luminosity peak at the top is a star and should be disregarded.

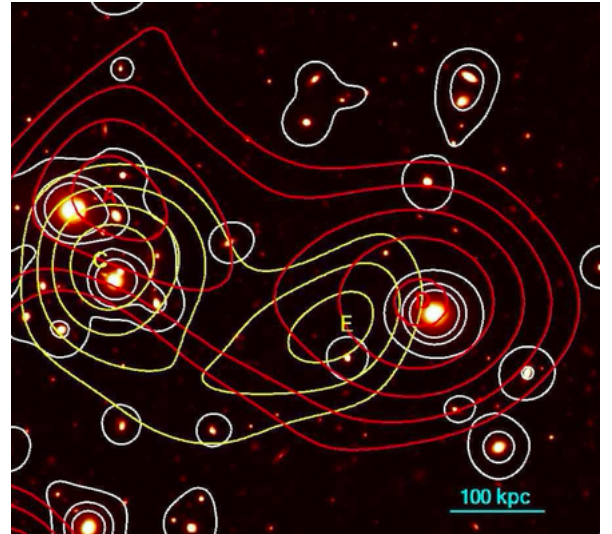
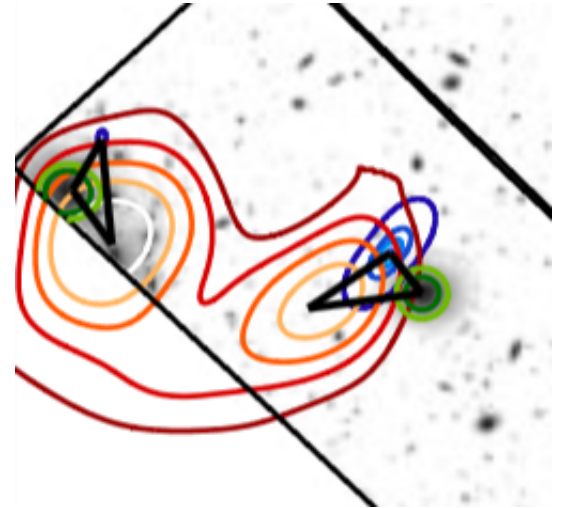


Figure 11. Top: H15 analysis of ZwCl 1234. Bottom: lensing (red), galaxy (white), and X-ray (yellow) contours from Dahle et al. (2013).

Table 1
Cluster Weights and Galaxy-DM Offsets

Weight (%)	δ_{SI} H15	δ_{SI} (kpc) Literature ^a	Name	§
16.7	66	Omit (M11)	Abell 2744 (west)	3.1
15.0	-19	80 (D13)	DLSCL J0916 (south)	3.2
10.1	36	No change	Abell 520-1	3.3
6.1	40	-4 (B09)	Bullet (east)	3.4
4.9	4	Omit (L14, S11)	MACS J2243 (east)	3.5
4.7	-7	Omit (Z11)	ZwCl 1358 (east)	3.6
4.7	81	Omit (J14a)	Abell 520-2	3.3
4.1	-151	-33 (B08)	MACS J0025 (west)	3.7
3.8	-32	21 (B09,R08)	Bullet (west)	3.4
3.4	-26	-4 (L14)	MACS J2243 (west)	3.5
2.9	22	Omit (J14a)	Abell 520-5	3.3
2.4	-150	Omit (J14b)	ACTCL J0102 (north)	3.8
2.1	2	No change	MACS J0417 (north)	3.9
1.8	28	No change	ZwCl 1234 (west)	3.10
1.7	84	Omit (C12,J14a)	Abell 520-3	3.3
1.6	-22	No change	Abell 520-4	3.3

^aReferences: B08 (Bradač et al. 2008); B09 (Bradač et al. 2009); C12 (Clowe et al. 2012); D13 (Dawson 2013); J14a (Jee et al. 2014a); J14b (Jee et al. 2014b); L14 (von der Linden et al. 2014); M11 (Merten et al. 2011); R08 (Randall et al. 2008); S11 (Schirmer et al. 2011); Z11 (Zitrin et al. 2011).

3.11. Summary

Table 1 summarizes the updates we recommend after reviewing the best available evidence from the literature. In four cases the literature is consistent with the offset (δ_{SI}) measured by H15; in five cases there is compelling evidence that the offset differs from that of H15; and in seven cases the H15 substructure either does not exist or does not support a clear association between a gas peak, a mass peak, and a galaxy peak. Although few of the H15 offsets are retained, this set of changes is the minimum necessary to bring the H15 offset catalog in line with the literature. In the next section we quantify the impact of these changes on the dark matter inference.

4. DARK MATTER INFERENCE

We begin with a brief recap of the H15 prescription for inferring σ_{DM}/m from the offset catalog. H15 approximate the probability density function (PDF) for each β_i as a Gaussian, as described in Section 2. They multiply these PDFs to find a PDF for $\langle\beta\rangle$ and then transform this into a PDF for σ_{DM}/m according to the relation $\sigma_{DM}/m = -\sigma_* \ln(1 - \beta)$, where σ_* is the characteristic cross-section (per unit mass) at which a halo becomes optically thick. They choose a central value of $\sigma_* = 6.5 \text{ cm}^2/\text{g}$ and “analytically marginalize” over the range $3.5 \leq \sigma_* \leq 9.5$ by quadrature addition to the second moments of the σ_{DM}/m PDF.

We prefer to avoid a Gaussian approximation for $p(\sigma_{DM}/m)$, and to marginalize numerically so that any non-Gaussian features can be preserved. We create a grid of models in the $(\sigma_{DM}/m, \sigma_*)$ parameter space, covering the region $(0 - 5, 3.5 - 9.5)$. For each point in the grid we multiply the β_i likelihoods as determined by the H15 prescription. We then marginalize over the σ_* axis to obtain a PDF, and take the cumulative sum to produce a cumulative distribution function (CDF). We present the CDF rather than the PDF because the CDF allows the reader to quickly read an upper limit at any desired confidence level, and allows for clearer comparisons between different constraints. Figure 12 shows the CDF for the reviewed subsample alone in black, for the full sample

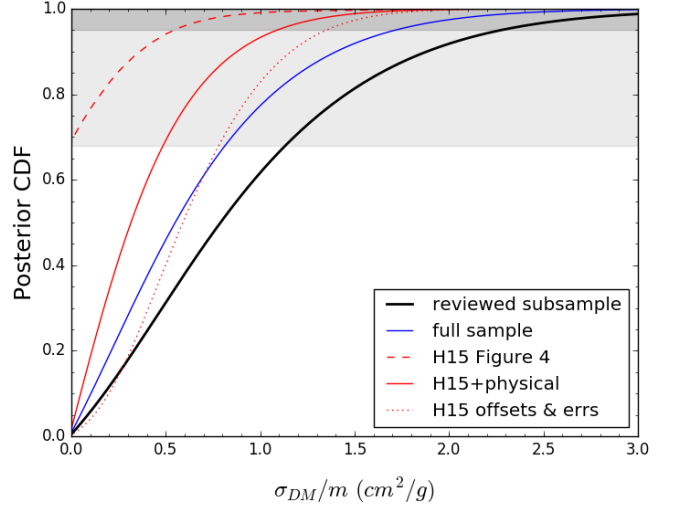


Figure 12. Constraints on σ_{DM} using the literature-reviewed offsets only (black) and in combination with the remaining H15 offsets (blue). Dashed red indicates the H15 constraint; solid red, the constraint with H15 offsets marginalized over physical models only; and dotted red, the constraint using H15 offsets and their uncertainties (rather than the default 60 kpc offset uncertainty in the H15 analysis). All variations on the H15 analysis lead to substantially relaxed upper limits.

(Table 1 plus the unreviewed H15 substructures comprising 15% of the total weight) in blue, and the CDF for a digitized version of H15 Figure 4 in dashed red. The H15 constraints become substantially looser after bringing the offsets into agreement with the literature, whether using the revised offsets alone (for which $\sigma_{DM}/m < 2.27 \text{ cm}^2/\text{g}$ at 95% confidence) or in combination with the remaining H15 offsets. None of the constraints shows tension with cold dark matter ($\sigma_{DM}/m = 0$) models.

Also shown are two additional CDFs we generated from the *unmodified* H15 offset catalog to illustrate the effects of certain analysis choices. First, note that H15 marginalized over the unphysical region of parameter space ($\sigma_{DM}/m < 0$) as well as the physical region ($\sigma_{DM}/m \geq 0$) over which we marginalize. Although we do not believe that one should marginalize over unphysical models to obtain confidence limits, we present both curves to display the impact of this choice. Taking the H15 catalog and marginalizing over the physical region only produces the solid red CDF in Figure 12. Comparing this to the dashed red CDF derived from H15 Figure 4, we see that excluding the unphysical region substantially relaxes the upper limits on σ_{DM}/m ; this follows directly from the fact that the H15 PDF *peaks* in the unphysical region. For all other CDFs presented in Figure 12, however, this choice has much less impact because the corresponding PDF peaks in the physical region. Including the unphysical region in the marginalization for the reviewed subsample, for example, moves the black CDF in Figure 12 to the left, but by much less than the difference between the blue and black curves, and is therefore omitted from the figure for clarity. In summary, our “reviewed subsample” and “full sample” constraints are relatively insensitive to the marginalization limits, but the H15 result is quite sensitive to this choice.

Second, H15 chose to ignore the varying uncertainties on their δ_{SI} measurements displayed in their Figure S2,

and instead assigned 60 kpc uncertainty to each δ_{SI} measurement in their analysis. Analyzing the H15 offsets with their individual uncertainties produces the dotted CDF in Figure 12; this relaxes the upper limits on σ_{DM}/m even more dramatically than did the change in marginalization. Furthermore, with individual uncertainties the PDF no longer peaks in the unphysical region: the steepest part of the CDF is well away from $\sigma_{DM}/m = 0$. Therefore, the choice of marginalization has little impact on constraints based on individual uncertainties.

We tested the sensitivity of the analysis to additional variations. As a reminder, our default analysis follows H15 in assigning 60 kpc uncertainty to each value of δ_{SI} —not because we endorse this procedure, but to demonstrate that a *minimal* set of changes to the H15 offsets and procedures yields substantially looser constraints. In one variation, we used the uncertainties displayed by H15 in their Figure S2 with our literature-based offsets. In a second variation, we inserted literature-based uncertainties where explicitly available, i.e. for the Bullet Cluster West (Randall et al. 2008, 25 ± 29 kpc.). In a third variation, we explored the sensitivity to gas mass correction by adding the mean 4.3 kpc correction back to each value of δ_{SI} . In all cases the constraint shifted by substantially less than the difference between the black and blue curves in Figure 12.

In summary, the revised offset catalog supports substantially relaxed upper limits compared to H15, even if we retain all the H15 analysis choices. Furthermore, the most likely value of σ_{DM}/m shifts from -0.25 to $\sim +0.25$ cm^2/g , indicating that the relaxed constraints are not merely a consequence of reduced sample size. A handful of striking examples illustrate why the central value shifted upward. The reviewed subsample included two extremely negative offsets ($\delta_{SI} \sim -150$ kpc), in MACS J0025 and ACTCL 0102. We found the former to be -33 kpc on closer inspection and the latter to be based on a spurious lensing peak. For two other highly weighted subclusters with $\delta_{SI} < 0$ in H15, DLSCL J0916 and the Bullet Cluster, previously published mass maps based on more extensive data and analysis revealed that in fact $\delta_{SI} > 0$. There were changes in the opposite direction as well, but they were less dramatic.

5. SUMMARY AND DISCUSSION

Adopting the H15 methodology but with corrections to their offsets based on the best available evidence in the literature and marginalizing only over physical models, we find a 95% confidence upper limit on σ_{DM}/m of $\lesssim 2$ cm^2/g , depending on whether one uses the high-quality subsample or the full sample. In other words, merging-cluster offsets do not yet support constraints tighter than the 1.25 cm^2/g at 68% confidence quoted by Randall et al. (2008). In this discussion we first defend the literature-review approach that led to this conclusion. Then, we explain why the H15 sample selection should lead readers to use even the revised constraints with caution. Finally, we discuss future prospects.

We predict two types of concerns readers may have with our approach:

- Bias: was evidence from the literature applied consistently without regard to the effect on the final result? It is impossible to remain ignorant

of the potential impact of a change in the offset when reviewing the H15 star-gas-DM geometry, because the geometry is so simple: if DM is self-interacting then it should be bracketed by the stars and the gas. We have attempted to minimize this concern by systematically examining the highest-weight substructures rather than the most negative or most suspect offsets. As *post facto* evidence that our review was not biased, we note that of the seven H15 substructures we omitted, five had positive offsets in H15, and only two had negative offsets. By itself, this should bring σ_{DM}/m down rather than up, barring complications such as the differing weights and sizes of the offsets. Of the changes to δ_{SI} that we recommend, the majority do go in the direction of lifting σ_{DM}/m from its H15 value, but the literature on these systems is so compelling that it speaks for itself.

- Inhomogeneity: the H15 catalog was produced in a mostly uniform way and uses only ACS data for photometry and lensing, but our corrections are based on a variety of data and analyses from the literature. While uniformity is a laudable goal, we do not believe it overrides the compelling evidence in the literature. Indeed, we believe the concern for uniformity is a major reason some of the H15 offsets are in error: single-band photometry is not sufficient to adequately characterize the mass and luminosity distribution of these systems.

These arguments suggest that any ill effects of bias and inhomogeneity are likely to be smaller than the beneficial effect of using more correct offsets.

We now turn to concerns about sample selection. The equation used by H15 to relate β to σ_{DM}/m was developed assuming only small ($\lesssim 30$ kpc) displacements between DM, galaxies and gas; Harvey et al. (2014) clearly shows how the analogy between galaxy and gas restoring forces (and hence the inferred drag force) breaks down quickly beyond 30 kpc displacements. Yet, many of the H15 offsets are very far outside this regime. Figure S2 of H15 readily shows that only five of the 72 substructures have both δ_{SI} and δ_{SG} within 30 kpc. Our updates have modestly reduced the spread of δ_{SI} values, but many violations of this approximation remain. In fact, the ensemble result is *driven* by substructures that violate the approximation, because the weight of each substructure is approximately proportional to δ_{SG}^2 (Equation 3).

The analogy between gas and self-interacting DM can break in other ways as well, for example if the gas is completely stripped at pericenter crossing. The analogy also breaks after the drag force (if any) subsides, for example well after pericenter as the subcluster travels to regions of lower and lower density. Subsidence of the drag force allows the gas and galaxies to each fall back to, and *through*, the DM. Recent SIDM simulations by Kim et al. (2016) clearly show the sign of the DM-galaxy offset changing as this happens. Separately, it has also been seen with gas in an effect known as the ram pressure slingshot: after ram pressure pulls the gas back from the center of the subcluster potential, gravity slings it forward (Markevitch & Vikhlinin 2007; Mathis et al. 2005; Hallman & Markevitch 2004; Ng et al.

2015). Because the maximum galaxy-DM displacement is smaller than the maximum gas-DM displacement, the two components cannot fall through the DM on the same timescale. Thus the ratio of displacements β cannot remain constant over time, and could even change sign at times. Averaging over a sample without regard to merger phase would then bias the inferred cross section low. We therefore suggest caution in interpreting even the revised constraints.

Although this conclusion is disappointing for current constraints, it does suggest that constraints from merging clusters could be tightened with a closer analysis of key systems including modeling the merger phase. We suggest that post-pericenter systems should be modeled with hydrodynamic simulations rather than with an analytical formalism. Cluster mergers can be competitive with other probes (e.g. Kahlhoefer et al. 2015), but more work remains.

Cluster mergers can also be used to test SIDM effects that cannot be modeled with a drag force; as noted by Kahlhoefer et al. (2014), the drag-force model maps well to frequent interactions with low momentum transfer, as in a long-range force. Infrequent interactions with large momentum transfer (as in hard scattering), in contrast, can eject particles from the cluster and is potentially observable as a decrease in the mass-to-light ratio; Randall et al. (2008) used the Bullet Cluster to constrain these models with an upper limit of $\sigma_{\text{DM}}/m < 0.7 \text{ cm}^2/\text{g}$ (68% confidence). This gives clusters a purpose beyond constraining the cross section at high velocity: if dark matter does interact with itself, comparing the two types of cluster constraints could point the way to a particle model of the interactions.

We thank Maruša Bradač, James Bullock, Bill Forman, James Jee, Felix Kahlhoefer, Manoj Kaplinghat, and Reinout van Weeren for helpful discussions. We especially thank David Harvey for being completely open with his code and his data, patiently answering our questions, and reviewing a complete draft. DW and NG were supported by NSF grant 1518246. Part of this work performed under the auspices of the U.S. DOE by LLNL under Contract DE-AC52-07NA27344.

REFERENCES

- Boylan-Kolchin, M., Bullock, J. S., & Kaplinghat, M. 2012, *MNRAS*, 422, 1203
- Bradač, M., Allen, S. W., Treu, T., Ebeling, H., Massey, R., Morris, R. G., von der Linden, A., & Applegate, D. 2008, *ApJ*, 687, 959
- Bradač, M., et al. 2009, *ApJ*, 706, 1201
- Brooks, A. 2014, *Annalen der Physik*, 526, 294
- Clowe, D., Markevitch, M., Bradač, M., Gonzalez, A. H., Chung, S. M., Massey, R., & Zaritsky, D. 2012, *ApJ*, 758, 128
- Cohen, T., Phalen, D. J., Pierce, A., & Zurek, K. M. 2010, *Phys. Rev. D*, 82, 056001
- Dahle, H., et al. 2013, *ApJ*, 772, 23
- Dawson, W. A. 2013, PhD thesis, University of California, Davis
- Dawson, W. A., et al. 2012, *ApJL*, 747, L42
- Elbert, O. D., Bullock, J. S., Garrison-Kimmel, S., Rocha, M., Oñorbe, J., & Peter, A. H. G. 2015, *MNRAS*, 453, 29
- Feldman, D., Kors, B., & Nath, P. 2007, *Phys. Rev. D*, 75, 023503
- Feng, J. L., & Kumar, J. 2008, *Phys. Rev. Lett.*, 101, 231301
- Hallman, E. J., & Markevitch, M. 2004, *ApJL*, 610, L81
- Harvey, D., Massey, R., Kitching, T., Taylor, A., & Tittley, E. 2015, *Science*, 347, 1462
- Harvey, D., et al. 2014, *MNRAS*, 441, 404
- Jauzac, M., et al. 2016, *MNRAS*, 463, 3876
- Jee, M. J., Hoekstra, H., Mahdavi, A., & Babul, A. 2014a, *ApJ*, 783, 78
- Jee, M. J., Hughes, J. P., Menanteau, F., Sifón, C., Mandelbaum, R., Barrientos, L. F., Infante, L., & Ng, K. Y. 2014b, *ApJ*, 785, 20
- Kahlhoefer, F., Schmidt-Hoberg, K., Frandsen, M. T., & Sarkar, S. 2014, *MNRAS*, 437, 2865
- Kahlhoefer, F., Schmidt-Hoberg, K., Kummer, J., & Sarkar, S. 2015, *MNRAS*, 452, L54
- Kaplinghat, M., Tulin, S., & Yu, H.-B. 2016, *Physical Review Letters*, 116, 041302
- Kim, S. Y., Peter, A. H. G., & Wittman, D. 2016, *ArXiv e-prints*
- Klasen, M., Pohl, M., & Sigl, G. 2015, *Progress in Particle and Nuclear Physics*, 85, 1
- Lindner, R. R., et al. 2014, *ApJ*, 786, 49
- Loeb, A., & Weiner, N. 2011, *Physical Review Letters*, 106, 171302
- Mann, A. W., & Ebeling, H. 2012, *MNRAS*, 420, 2120
- Markevitch, M., Gonzalez, A. H., Clowe, D., Vikhlinin, A., Forman, W., Jones, C., Murray, S., & Tucker, W. 2004, *ApJ*, 606, 819
- Markevitch, M., Govoni, F., Brunetti, G., & Jerius, D. 2005, *ApJ*, 627, 733
- Markevitch, M., & Vikhlinin, A. 2007, *Phys. Rep.*, 443, 1
- Mathis, H., Lavaux, G., Diego, J. M., & Silk, J. 2005, *MNRAS*, 357, 801
- Medezinski, E., Umetsu, K., Okabe, N., Nonino, M., Molnar, S., Massey, R., Dupke, R., & Merten, J. 2016, *ApJ*, 817, 24
- Menanteau, F., et al. 2012, *ApJ*, 748, 7
- Merten, J., et al. 2011, *MNRAS*, 417, 333
- Newman, A. B., Treu, T., Ellis, R. S., & Sand, D. J. 2013a, *ApJ*, 765, 25
- Newman, A. B., Treu, T., Ellis, R. S., Sand, D. J., Nipoti, C., Richard, J., & Jullo, E. 2013b, *ApJ*, 765, 24
- Ng, K. Y., Dawson, W. A., Wittman, D., Jee, M. J., Hughes, J. P., Menanteau, F., & Sifón, C. 2015, *MNRAS*, 453, 1531
- Peter, A. H. G., Rocha, M., Bullock, J. S., & Kaplinghat, M. 2013, *MNRAS*, 430, 105
- Randall, S. W., Markevitch, M., Clowe, D., Gonzalez, A. H., & Bradač, M. 2008, *ApJ*, 679, 1173
- Rocha, M., Peter, A. H. G., Bullock, J. S., Kaplinghat, M., Garrison-Kimmel, S., Oñorbe, J., & Moustakas, L. A. 2013, *MNRAS*, 430, 81
- Sand, D. J., Treu, T., Ellis, R. S., Smith, G. P., & Kneib, J.-P. 2008, *ApJ*, 674, 711
- Schirmer, M., Hildebrandt, H., Kuijken, K., & Erben, T. 2011, *A&A*, 532, A57
- Sifón, C., et al. 2013, *ApJ*, 772, 25
- von der Linden, A., et al. 2014, *MNRAS*, 439, 2
- Zavala, J., Vogelsberger, M., & Walker, M. G. 2013, *MNRAS*, 431, L20
- Zitrin, A., Broadhurst, T., Coe, D., Liesenborgs, J., Benítez, N., Rephaeli, Y., Ford, H., & Umetsu, K. 2011, *MNRAS*, 413, 1753
- Zitrin, A., Menanteau, F., Hughes, J. P., Coe, D., Barrientos, L. F., Infante, L., & Mandelbaum, R. 2013, *ApJL*, 770, L15